LIGO-T970239-A-D

HYTEC-TN-LIGO-14a
02/18/97
revision *a*, 04/09/97

LIGO Coil Springs Test Report

Eric Ponslet
February 18. 1997
Revision *a*, April 9, 1997

Abstract

This report summarizes results from static and fatigue tests, dynamic stiffness and damping evaluations, and visual inspections of the LIGO coil springs.

HYTEC Inc.
110 Eastgate Dr., Ste 100
Los Alamos, NM 87544
(505) 662-0080 / Fax (505) 662-5179

LIGO PROJECT

Table of Contents

1. Undamped Coil Prototypes (UC01, UC02, UC03)

1.1 Coil and Seats

An "undamped" test coil (with solid Viton core) is shown in Fig. 1, supported on temporary molded epoxy seats. The measured coil parameters are as follows:

Total # of turns	4
# unsupported turns	2.5
mean coil diameter	52.4 mm
pitch	14.0 mm
mean cross section OD	9.51 mm
mean cross section ID	7.79 mm

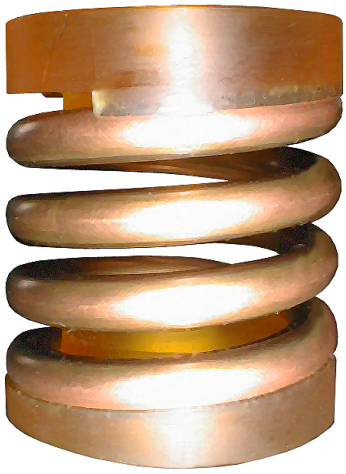

Figure 1: Undamped coil prototype and epoxy seats.

In spite of special tooling used in the coiling operation, the cross section is not perfectly circular as shown in Fig. 2.

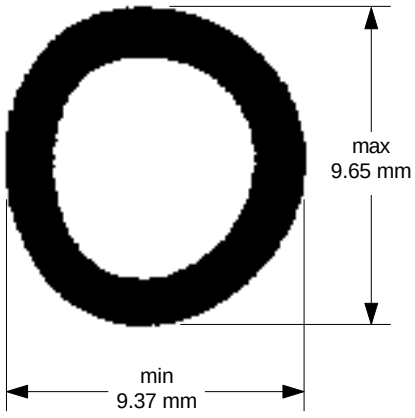

Figure 2: Coiled tube cross section typical of undamped prototypes UC01, UC02, and UC03 (from digitized thin slice).

Three coils were available for testing (UC01, UC02, UC03) in addition to a preprototype (UC00) used for test setup adjustments and trials. Coils UC02 and UC03 were baked in air at 310°F for 1 and 3 hours respectively in an attempt to partially relieve coiling stresses[1], while UC01 was left unbaked.

1.2 Static and Fatigue Testing

1.2.1 Experimental Setup

All three prototypes were tested in a hydraulic MTS testing machine to measure spring rate, permanent set, and load capacity. The experimental setup is shown in Fig. 3. The spring is resting between two epoxy seats which are held centered on the fixed and moving ends of the testing machine. The fixed end (top) is equipped with a 5 kN load cell and the moving end (bottom) with an embedded LVDT displacement sensor. All tests were performed in displacement control mode.

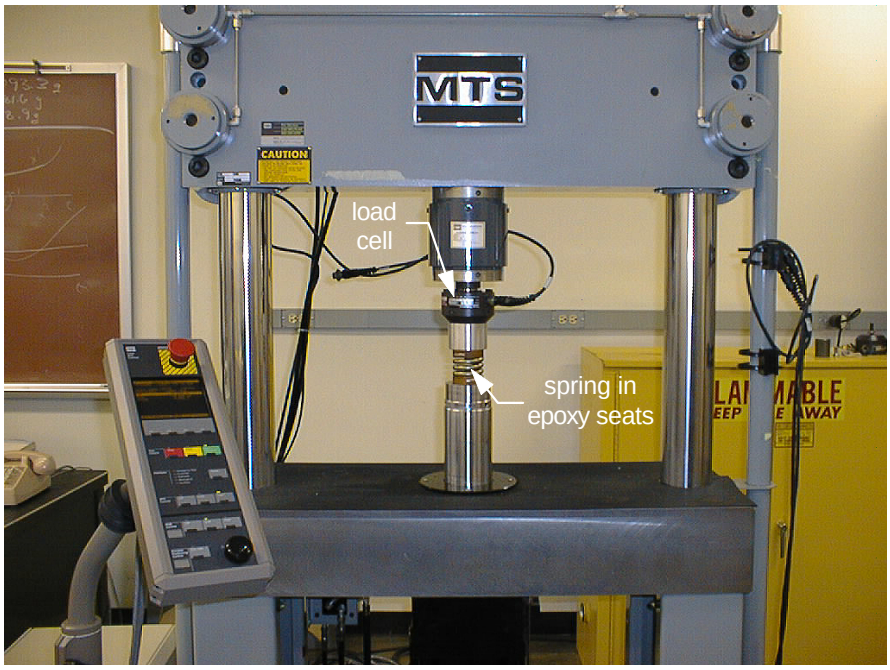

Figure 3: Static and fatigue test setup.

1.2.2 Test Procedures

Before the actual tests, the following adjustments were made:

- with adapters and seats in place (but no spring), reset load cell output to zero.
- using a dummy spring (pre-prototype UC00), manually adjust the machine to a preload position giving a load cell output of about 25 lbs; reset the LVDT deflection output to zero.
- measure length between loading surfaces: L_0 = 2.865” = 72.77 mm.
- using a sheet of paper as a feeler (about .004” / 0.1 mm thick), move machine by hand until contact between successive coils is achieved. Measure displacement:

δ_{solid} = -0.493" (12.52 mm) and infer distance between loading surfaces: $L_{solid} = L_0 + \delta_{solid}$ = 2.372" (60.25 mm).

All 3 springs were then submitted to the following automatic sequence:

1. *Initial Static Loading (measure permanent set)*
    - place spring in machine and bring machine to zero deflection (which gives about 25 lbs preload). Note that the prototype springs have never been loaded before this test.
    - hold for 5 seconds.
    - ramp load from 0 to -0.262" (6.65 mm), at 0.05 in/sec (1.27 mm/sec), ramp unload back to 0 at same rate, repeat 4 times. Acquire and store time, displacement, and load at .0025 second intervals (400 data/second sampling rate).
    - hold for 5 seconds.
    - ramp load from 0 to -0.330" (8.38 mm), at 0.05 in/sec (1.27 mm/sec), ramp unload back to 0 at same rate, repeat 4 times. Acquire and store time, displacement, and load at .0025 second intervals (400 data/second sampling rate).
    - hold for 5 seconds.
    - ramp load from 0 to 95% δ_{solid} = -0.470" (11.94 mm), at 0.05 in/sec (1.27 mm/sec), ramp unload back to 0 at same rate, repeat 4 times. Acquire and store time, displacement, and load at .0025 second intervals (400 data/second sampling rate).
    - hold for 5 seconds.
2. *Cyclic loading to 95% solid (detect fatigue and further set)*
    - sinusoidal cyclic loading between 0 and 95% δ_{solid} = -0.470" (11.94 mm), at 0.5 in/sec (12.7 mm/sec) peak rate, repeat 2000 times. Acquire and store time, displacement, and load for each minimum and maximum in displacement (6 data points per cycle).
    - hold for 5 seconds.
3. *Static testing (measure spring rate)*
    - repeat exact same procedure as 1.

1.2.3 Results

The time histories of load and displacement for initial loading of spring UC01 is shown in Fig. 4 for illustration.

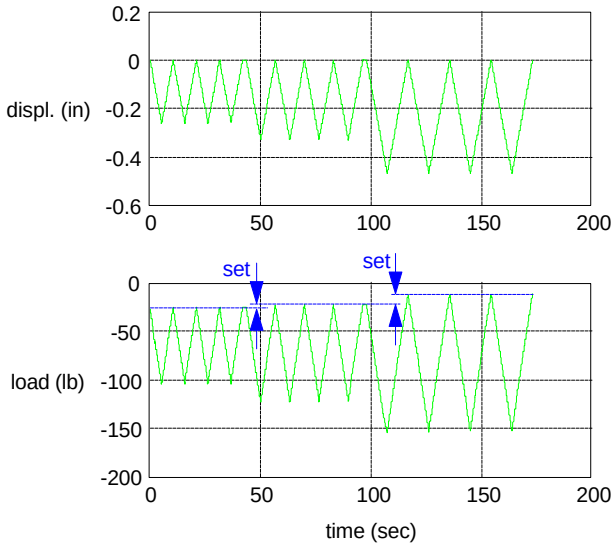

Figure 4: Time histories of initial static loading of coil UC01.

Fig. 5 shows results for all 3 springs as load/deflection curves. Permanent plastic set is clearly visible at each load increase and for all 3 springs. The results show little difference between the 3 springs: it appears that the baking relaxes the springs slightly, increasing their free length before they are loaded. However, the baked springs (UC02, UC03) also set more than the unbaked one (UC01). The final result is that, after being loaded to solid length a couple times, all 3 springs' load-deflection curves look essentially identical; total set is about 0.06" (1.5 mm) after loading to solid length. These results indicate that the baking operation is not needed. However, all springs may have to be preset by compressing them to solid length a few times before use.

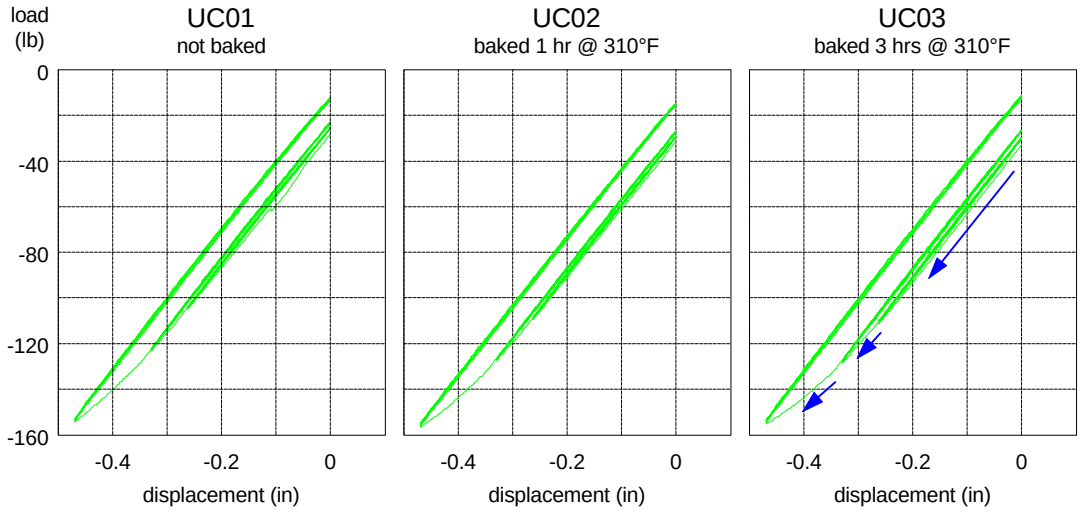

Figure 5: Initial static loading of undamped coil prototypes.

Load-deflection curves for 2000 cycles are shown in Fig. 6. Note a small amount of additional set (which occurs during the first couple hundred cycles). Finally, the static

test was repeated after cyclic loading and the corresponding curves are shown in Fig. 7. Note that no further set is observed and the behavior of the 3 springs is very similar.

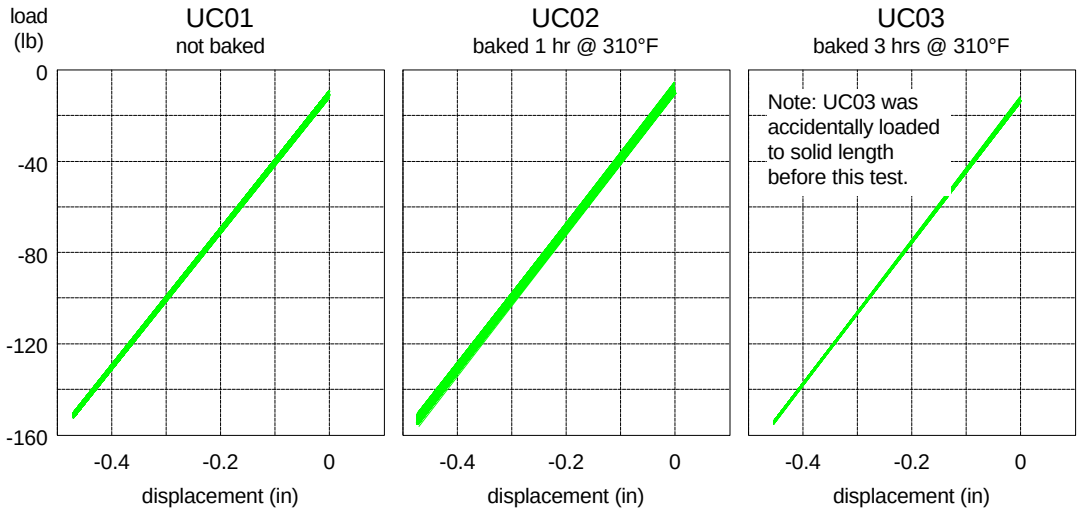

Figure 6: Cyclic loading of undamped coil prototypes (2000 cycles from 0 to 95% solid).

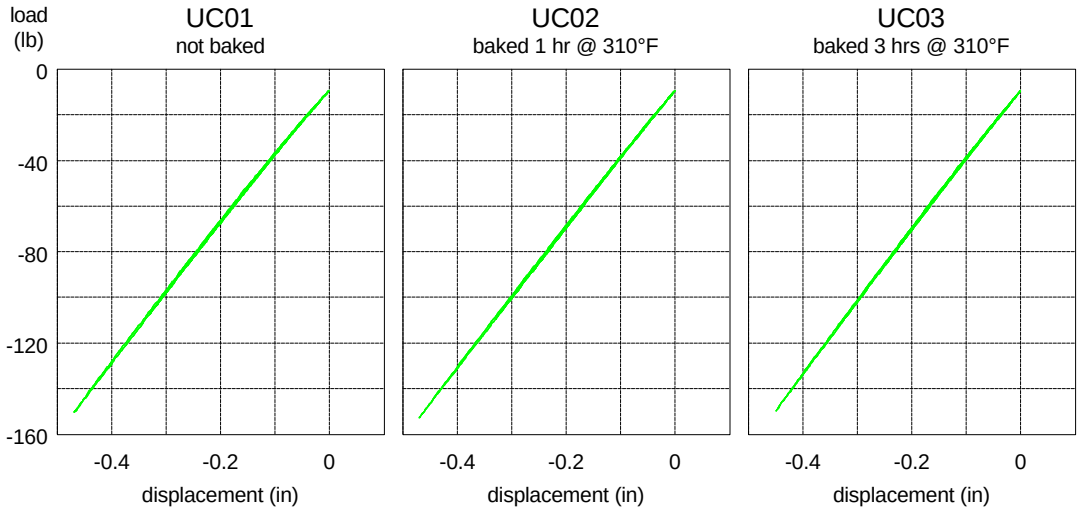

Figure 7: Static loading of undamped coil prototypes after cyclic loading.

The springs' static axial stiffnesses are then extracted form the results of Fig. 7 by linear fit of the load-displacement curve in the 90+ lbs range (tangent stiffness around nominal preload). This leads to the following numbers:

UC01	55033. N/m (314.3 lb/in)
UC02	54794. N/m (312.9 lb/in)
UC03	56563. N/m (323.0 lb/in)
mean measured static axial stiffness	55463. N/m (316.7 lb/in)

1.3 Evaluation of number of effective free coils

The coils do not behave as if they were perfectly clamped at their exit point from the seats. Therefore, analysis of the coil spring has one unknown parameter: the effective number of active coils. This number must be between 2.5 (number of unsupported coils) and 4 (total number of coils). All other parameters of the analysis are either geometric dimensions or material properties. The number of active coils can then be adjusted via a simple line search technique so that the analytical value of axial stiffness matches the measured value. This process leads to

effective number of active coils	3.16.
static stiffness - analytical prediction	55463 N/m (316.7 lb/in)

This number is then used for analysis of any spring that uses the same type of epoxy seats (like the damped coil prototype of the next two sections).

2. Damped Coil Pre-prototypes (DC00 and earlier)

2.1 Coil and Seats

The damped coil prototype DC00 (Fig. 8) differs in mean coil diameter from its undamped counterpart UC00. Other dimensions are very similar except of course for the internal structure which includes the multi-layer damping system (section 2.2). Best estimates of actual outside dimensions are listed below. Also, because this spring is made of a softer temper of phosphor bronze (1/4 hard instead of the ¾ hard design temper, for reasons of material shortages), it was not tested for static load capacity.

Total # of turns	4
# unsupported turns	2.5
# active coils	3.16 (see section 1.3)
mean coil diameter	59.0 mm
pitch	14.0 mm
mean cross section OD	9.52 mm

Figure 8: Damped coil pre-prototype DC00 in its molded epoxy seats.

2.2 Internal Structure

This damped coil contains a multi-layer internal damping structure[2]. A photograph of an actual cross section is shown in Fig. 9.

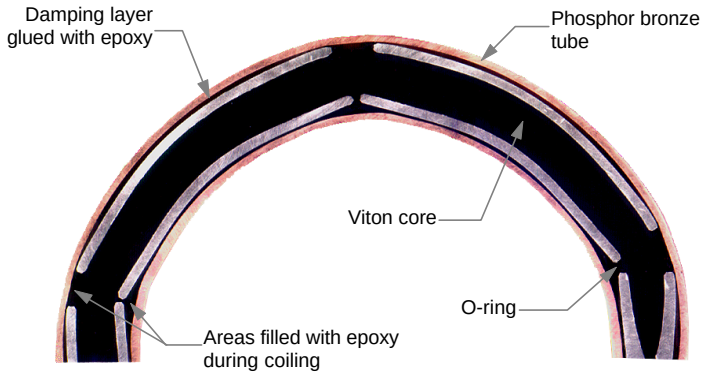

Figure 9: Section through early pre-prototype coil showing internal structure (the apparently V shaped aluminum piece at the bottom right hand side is only due to the fact that the section is not going through the coil centerline at that point).

The inside of the phosphor bronze outer tube is filled with (from the inside out) a viton core, a series of aluminum tube sections separated longitudinally by rubber O-rings, a thin layer of epoxy glue, a layer of DYAD 606 damping material, and another thin layer of epoxy. The entire fabrication of the spring is completed before the epoxy has time to set. This allows all voids that form during coiling to be filled with epoxy (in particular the fairly large gaps between the aluminum tubes at the outside of the coil). The rubber O-rings prevent the aluminum sections from making contact with each other after coiling. Note that the aluminum tube sections do not completely conform to the coiling of the outside tube and tend to crush the damping layer near their outside edge. This imperfection is not expected to have a large effect on performance; however, there is a concern that over time, the aluminum might locally "wear" through the damping sheet, creating metal to metal contact which could lead to creaking noise problems. Best estimates of actual (average) inside dimensions are given below:

Length of each aluminum tube	35.3 mm
Phosphor bronze tube OD	9.52 mm
Phosphor bronze tube ID	7.80 mm
Aluminum tube OD	6.74 mm
Aluminum tube ID	4.90 mm

2.3 Rough Estimation of Axial Loss Factor (Free Decay Tests)

To get a first idea of axial loss factor in the damped prototype, we measured free decay accelerograms using the setup of Fig 10. The spring is resting in its epoxy seats on the load frame of an Instron testing machine (used only for its high stiffness). The top seat is supporting an aluminum loading block to which a 3/8" all-thread is attached. The all-thread runs free through holes in the bottom seat and the support beam and carries weights at its free end. The rod-weight system provides static stability to the precompressed spring and leads to a very low frequency pendulum mode (about 0.5Hz).

An accelerometer is mounted on the aluminum block on top of the spring. Initial condition is created manually, by pressing down on the aluminum block. The accelerometer signal is recorded on a digital storage oscilloscope.

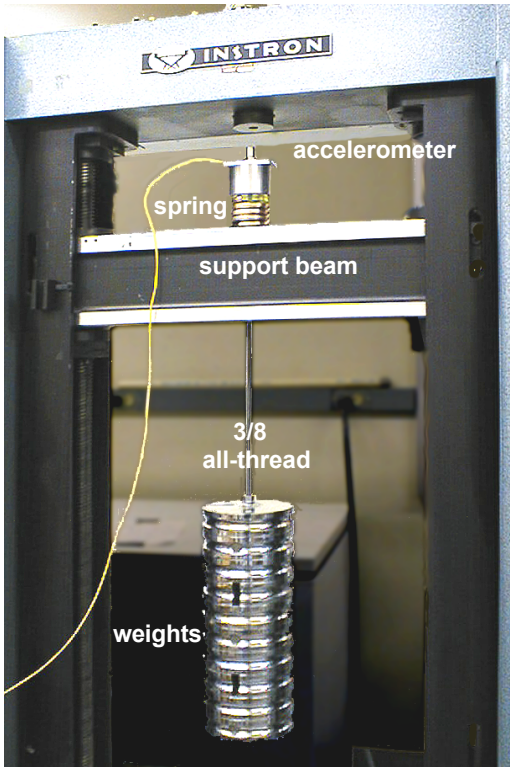

Figure 10: Free decay test setup for evaluation of axial loss factor.

The frequency of the vertical mode ranges from about 5 to 10 Hz, depending on the amount of mass suspended on the rod. There was unfortunately a bending mode in the rod at an estimated frequency between 4 and 6 Hz which may have influenced apparent damping in that frequency range (see results). Results from an FEM model of the test setup (Fig. 11) confirm this suspicion.

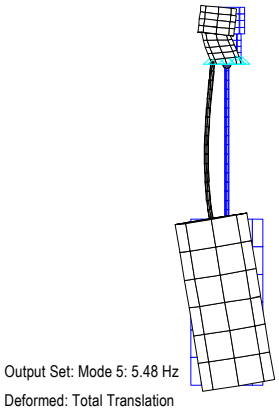

Figure 11: FEM analysis of free decay test setup; bending mode at 5.5 Hz.

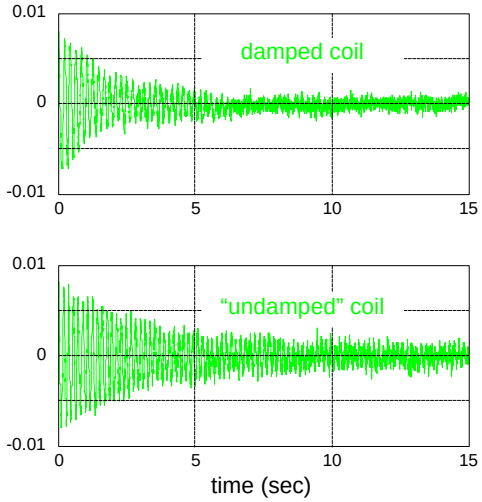

Figure 12: Free decay acceleration traces; damped coil prototype DC00 (top) compared to undamped coil DC01 (bottom).

Measurements were first taken on an undamped coil (UC01) with 100 lb mass, then on the damped coil pre-prototype (DC00) using masses of 20, 50, and 100 lb. The tests on the damped coil were repeated 3 times for each value of the mass. Loss factors and natural frequencies were extracted through least square fit of the accelerograms. Those values are shown in Fig. 13 and compared to analytical predictions. Note the sharp increase in observed damping around 5 Hz which may be due to energy exchange with the bending mode.

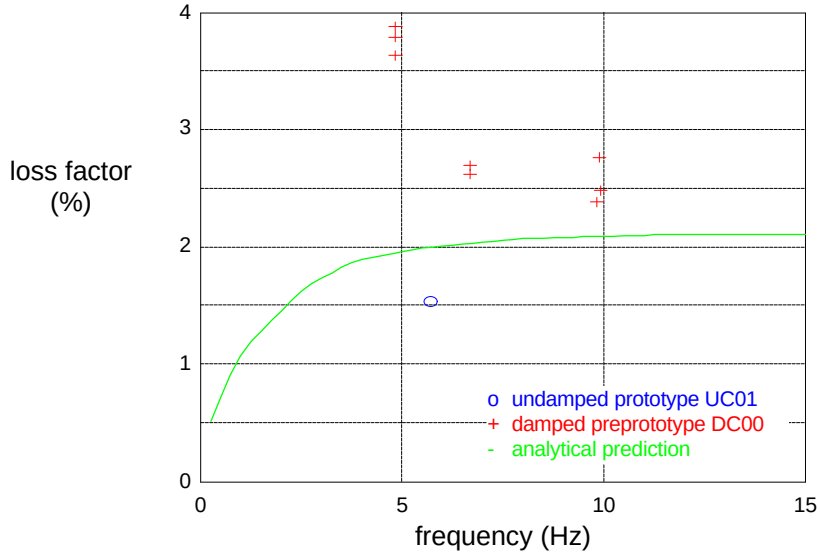

Figure 13: DC00 damped coil preprototype - free decay tests with rod; measured VS analytical loss factors.

In an attempt to eliminate the parasitic bending mode, similar tests were repeated with the modified setup of Fig. 14. The rod has been replaced with a soft cable, eliminating any bending modes from the system and also making the setup more forgiving (self-centering).

Figure 14: Modified free decay test setup for evaluation of axial loss factor; threaded rod replaced with cable to eliminate parasitic bending mode.

This time both the undamped (UC00) and damped (DC00) prototypes were tested 3 times for each amount of mass (25, 50, 75, and 100 lbs). Frequencies and loss factors were extracted through non-linear least square fit on the accelerograms and the results are shown in Fig. 15.

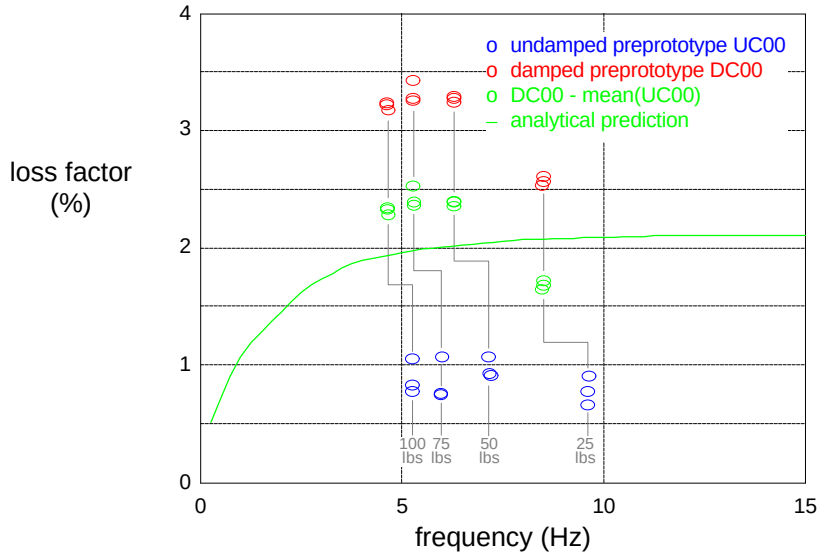

Figure 15: DC00 damped coil preprototype - free decay tests with modified setup (cable); measured VS analytical loss factors.

Note first that the resonant frequencies of the damped and undamped coils do not match because of the difference in mean coil diameter. Loss factors in the "undamped" coil (blue circles) averages about 0.88%, roughly independent of preload. Assuming negligible change in stiffness from the undamped to the damped coil, loss factors are roughly additive; the figure also shows the measured loss in the damped coil corrected by 0.88% (green plus signs). This corrected loss can be attributed entirely to the internal structure of the damped spring and is compared to analytical predictions. Overall, these results appear in good agreement with analysis. However, the damping observed with 25 lb preload is unexpectedly lower than with larger preloads. We might speculate that with small preloads the coil may not be tightly in contact with its epoxy seat, leading to erratic variations in damping; however, the undamped coil results do not clearly show evidence of this.

3. Damped Coil Prototypes (DC01, DC02, DC03)

3.1 Coils

The encouraging results from axial Q tests on the damped coil preprototype convinced us to produce 3 more prototypes (DC01, DC02, and DC03, shown in Fig. 16. Because rubber seats were not yet available, we manufactured molded epoxy seats for these 3 springs as well; figure 16 shows the three coils in those epoxy seats. This section presents results both with Epoxy and Fluorel rubber seats. Again because of material shortage, only 2 of those 3 prototypes (DC01 and DC02) are made from the ¾ hard phosphor bronze tube. The third one is made of a ½ hard temper. However, the differences in temper should have no influence on Young's modulus or loss factor of the complete spring.

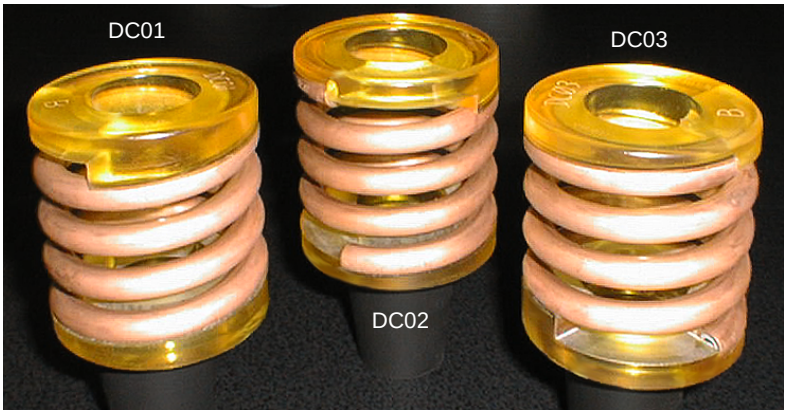

Figure 16: Coil spring prototypes DC01, DC02, DC03 ready to be tested with temporary epoxy seats.

3.2 Internal Structure

To try and improve on the local "crushing" of the damping layer visible in DC00, we machined aluminum tube sections with the last 6.4 mm (¼") at each end tapered down to about half the wall thickness. Figure 17 shows a photograph of a cross section through a

coil made with those modified aluminum tubes. Clearly, the taper has eliminated much of the "crushing" of the damping layer at the outside edge of the aluminum tubes. However, the tapers at the ends of the aluminum tubes lets the spacer O-rings slip over the tubes, which results in very little (if any) axial separation between the aluminum sections at their inside edge.

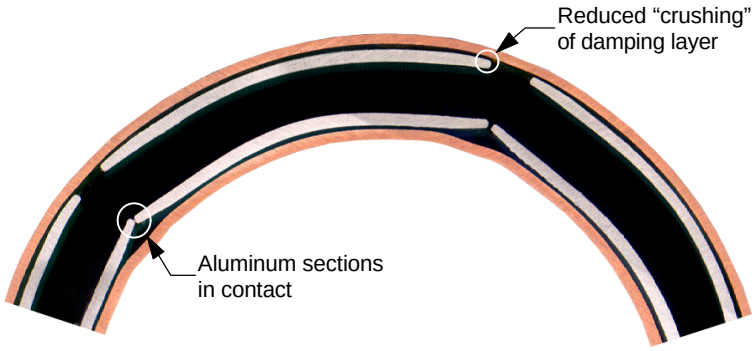

Figure 17: Section through prototype coil DC02 showing internal structure (note the tapered aluminum tube sections).

4. Experimental Results on Epoxy Seats

4.1 Axial Loss Factor (Free Decay Tests)

The tests described in Section 2.3 were repeated on these 3 coils, using the setup of Fig. 14 and a more sensitive accelerometer. A closeup of one of the springs loaded to 100 lbf is shown in Fig. 18.

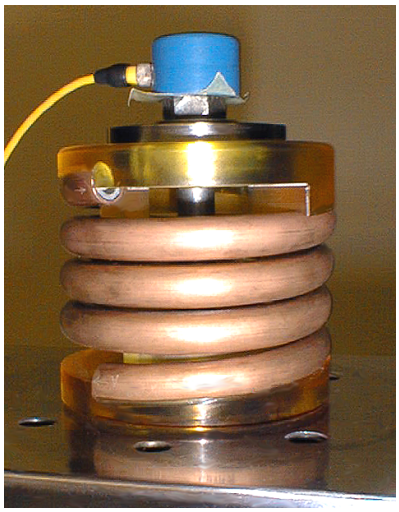

Figure 18: Spring prototype being tested for axial damping (free decay) with 100 lbf compressive load.

Tests were performed with 25, 50, 75, and 100 lbs masses and each measurement was repeated twice. A least square fit in the time domain was used to extract frequencies and

loss factors. The results are shown in Fig. 19 and compared to analytical results as well as measured values on the pre-prototype DC00.

Note that these new results do not exhibit the sharp reduction in damping at 25 lbs preload as observed on DC00. Also note that repeated measurements in the same conditions produce very repeatable values of loss factors. However, the three springs are not producing very consistent amounts of damping (almost 30 % difference). It also appears that these 3 springs have less damping than the pre-prototype although the difference may be too small to be really significant. If a difference really exists, it may be due to direct contact between some aluminum sections and/or to the locally increased thickness of the damping layer at the inside of the coil due to chamfering of the aluminum sections. Further refinements to the design and manufacturing processes should shed some light on this question.

Finally, the results of Fig. 19 do not confirm (or clearly infirm) the frequency dependence of the loss factor predicted by analysis. In particular they do not provide any confirmation of the sharp decrease in damping at low frequency. Direct measurements at lower frequencies are clearly needed to clarify this point.

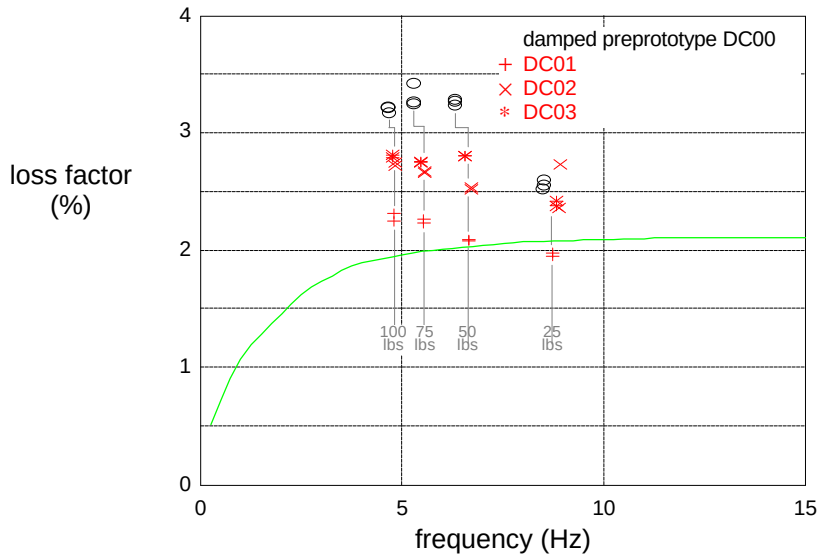

Figure 19: DC01, DC02, and DC03 damped coil prototypes - free decay tests with modified setup (cable); measured VS analytical axial loss factors. Values for DC00 are also included for comparison.

4.2 Static and Fatigue Testing

The procedures are identical to those described in section 1.3, with the following exceptions:

- The springs are preloaded to about 20 lbs before the LVDT displacement sensor is reset to zero.
- For the static tests, the springs are cycled 4 times from 0 to 3 mm, then 0 to 6 mm, then 0 to 9 mm
- For the fatigue tests, the number of cycles was reduced to 1000 and the springs are deflected from 0 mm (20 lb preload) to 10.9 mm (almost solid).

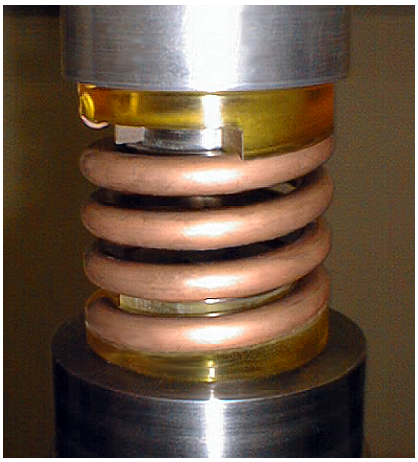

Figure 20: Damped coil spring prototype in MTS testing machine.

Figure 21 shows the load deflection curves for initial loading (the springs were never loaded before). Some set is visible, but to a lesser extent than observed on the undamped prototypes. This is the result of the larger coil diameter, which results in lower shear stress levels in the PhBr tubes. Also, the ½ hard coil may be setting slightly more than the other two (3/4 hard), although the difference may not be large enough to be significant.

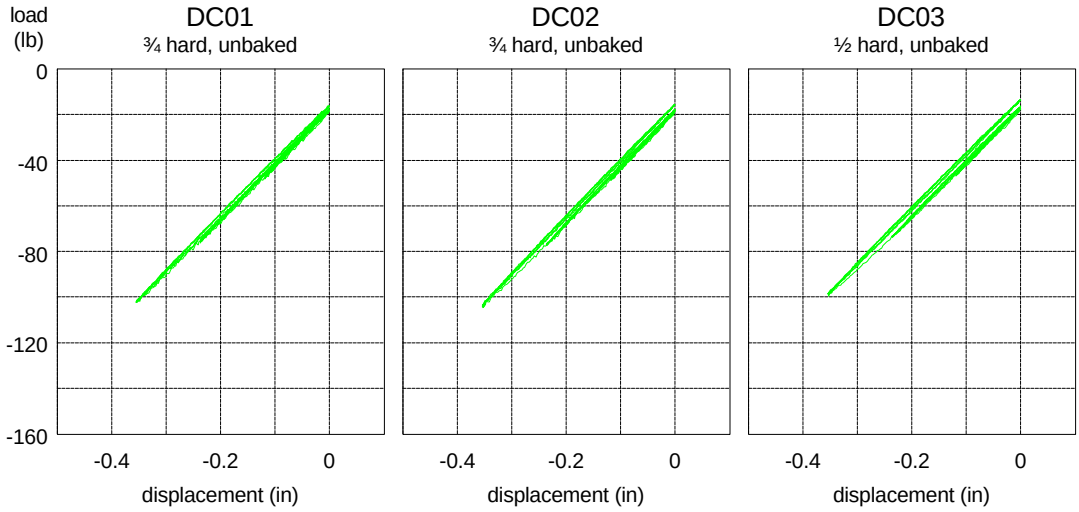

Figure 21: Initial static loading of damped coil prototypes.

The load displacement curves for 1000 cycles at full deflection are shown in Fig. 22. A very small amount of additional set is observed. Finally, static testing is repeated after the cycling and results in the curves shown in Fig. 23. No significant set or hysteresis is visible (these are very slow deformation rates so that any hysteresis could only be attributed to slippage or creep effects, not viscoelastic damping).

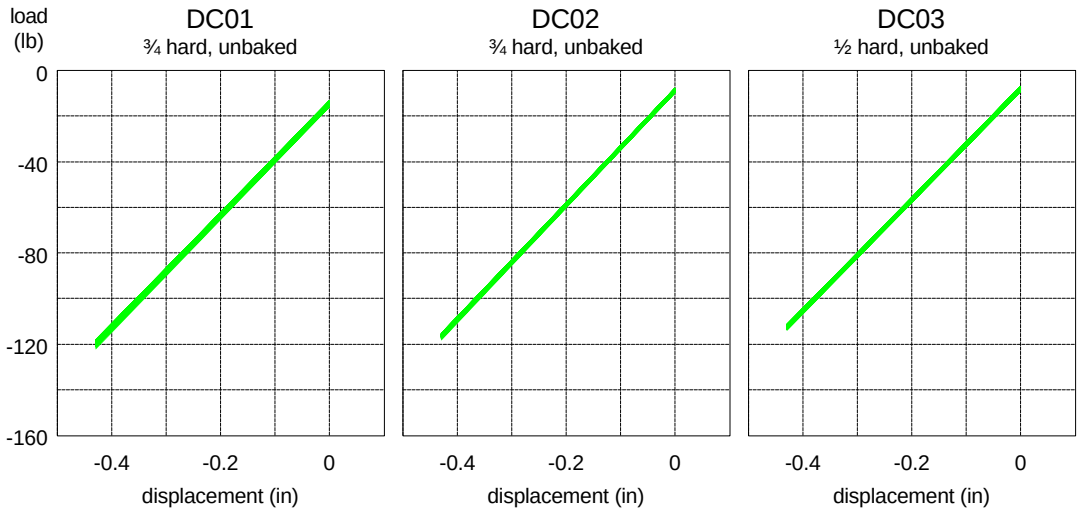

Figure 22: Cyclic loading of damped coil prototypes (1000 cycles from 0 to approximately 95% solid).

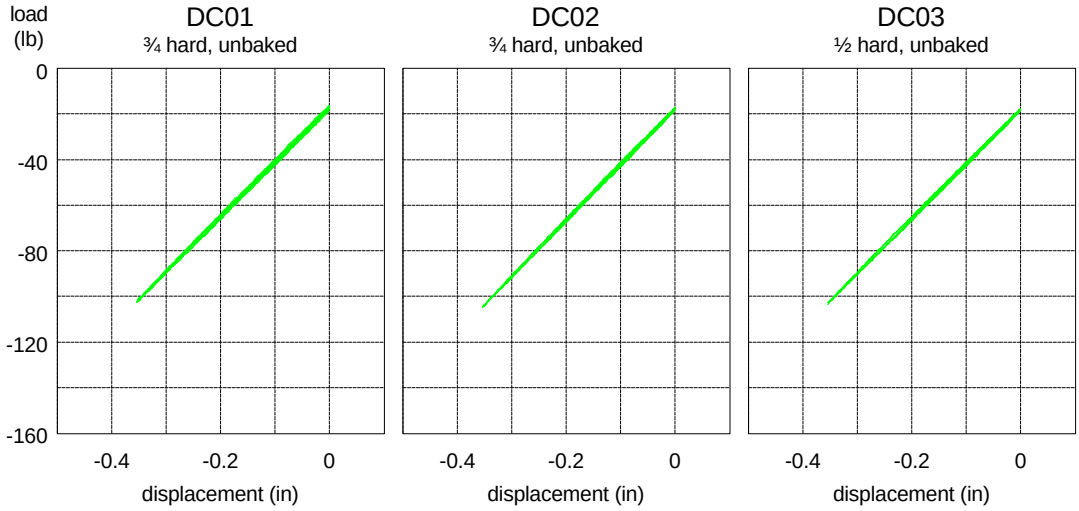

Figure 23: Static loading of damped coil prototypes after cyclic loading.

The springs' static axial stiffnesses are then extracted from the results of Fig. 23 by linear fit of the load-displacement curve in the 90+ lbs range (tangent stiffness around nominal preload). These numbers are listed below and compared to analytical predictions based on the number of active coils (3.16) identified from static tests on the smaller diameter undamped coil (see section 1.3).

DC01	42799. N/m (244.4 lb/in)
DC02	43429. N/m (248.0 lb/in)
DC03	42536. N/m (242.9 lb/in)
mean static axial stiffness	42921. N/m (245.1 lb/in)
analytical (3.16 turns)	40981. N/m (234.0 lb/in)

4.3 Single Stage Stack Testing

To obtain some data on shear behavior of the springs, a single stage platform was tested at Sandia National Laboratories. The platform is a 36"×48" ×1.25" anodized aluminum plate, instrumented with 4 triaxial accelerometers close to its corners. The plate alone weighs 200.5 lbs. Four 25 lb steel masses and a smaller counterweight (see photograph in Fig. 24) are bolted to it to bring its mass to 300 lbs and its center of mass to its geometric centerpoint. The resulting platform is supported on our 3 coil prototypes, symmetrically arranged around the center (see Fig. 25). This system is resting on a solid aluminum base weighing more than 4000 lbs.

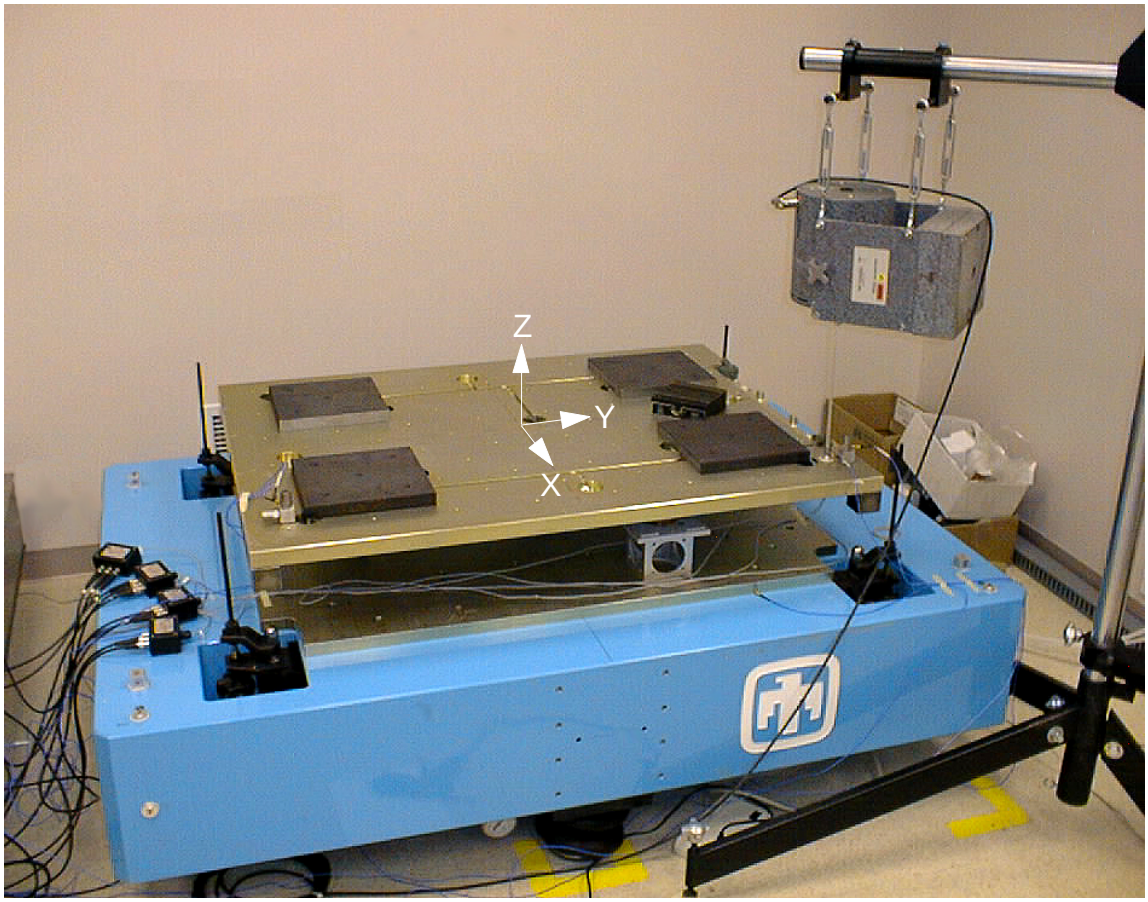

Figure 24: Single stage platform test setup (platform weighs 300lbs and is supported by 3 springs DC01, DC02, DC03).

Figure 25 shows a close up of one of the springs supporting the platform. Note how the spring is loaded close to solid length with 100 lbs. This minimizes the number of springs required in the stack, maximizing performance.

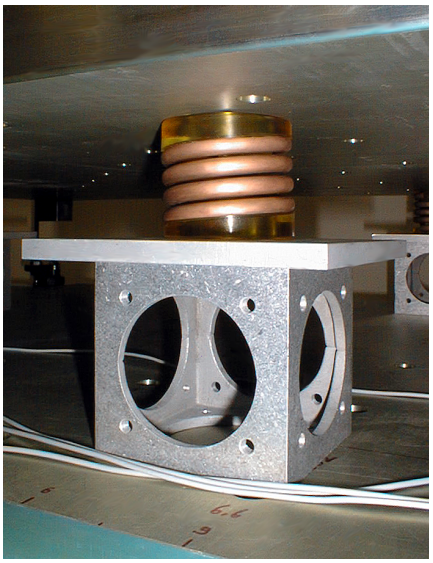

Figure 25: Close-up on a coil spring in the single stage platform test setup (aluminum base block provides clearance to lifting system).

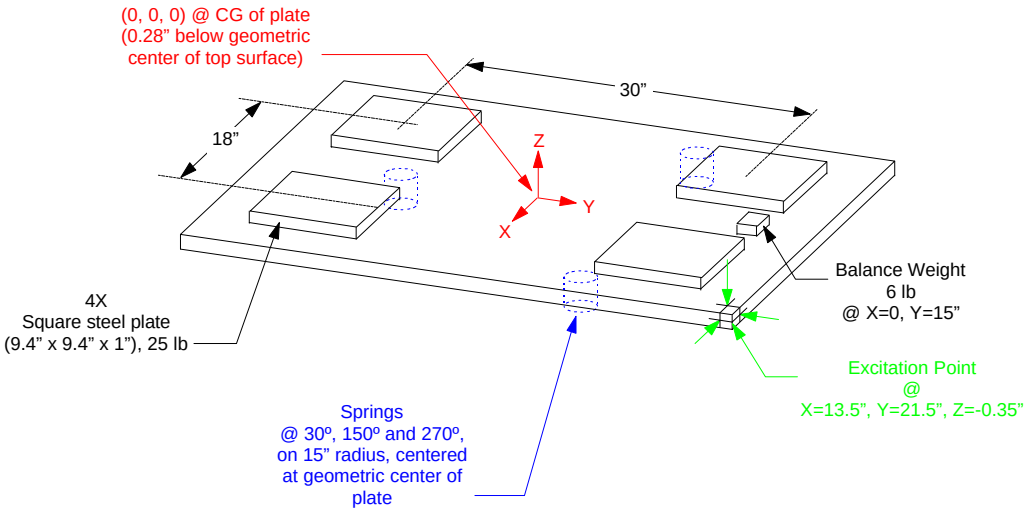

Figure 26: single stage platform test setup.

Three sets of 12 transfer functions each were measured on that platform. For the first set, we excited a corner of the table in the X direction (white noise) and measured responses at the 4 triaxial accelerometers. The second and third set were similarly measured for excitations in the Y and Z directions. These three sets of transfer functions were then processed independently with IDEAS to extract natural frequencies, loss factors, and mode shapes. In all cases, comparisons of experimental transfer functions with the models fitted by IDEAS showed extremely good match. Those results are summarized in Table 1.

Mode #	Nat. Frequency [Hz]			Loss Factor h = 2V[%]			Quality Factor Q = 1/h			Mode Shape
	Excitation dir.			Excitation dir.			Excitation dir.			
	X	Y	Z	X	Y	Z	X	Y	Z	
1	3.63	3.64	3.64	2.94	1.68	2.01	34	60	50	rocking around X
2	4.95	*	4.96	1.88	*	1.57	53	*	63	rocking around Y
3	5.01	5.01	5.02	2.15	2.67	1.75	47	38	57	up/down along Z
4	6.14	6.15	6.16	1.53	1.44	1.56	65	69	64	twist around Z
5	7.14	7.15	7.17	1.63	1.61	1.63	61	62	62	shear along Y
6	7.41	7.42	7.44	1.58	1.48	1.59	63	68	63	shear along X

* not observed

Table 1 Modal parameters extracted from tests with each excitation direction (from IDEAS modal identification).

Mode number 4 (6.15 Hz average) is a pure twist of the table around its vertical axis, involving almost only shear deformations in the springs. This mode can therefore be used to extract shear stiffness and loss factor at 6.15 Hz according to (small damping approximation)

$$k_{shear}(6.15\text{ Hz}) = \frac{4\pi^2 (6.15)^2 J_{zz}}{3d^2}, \qquad (1)$$

where J_{zz} is the moment of inertia of the platform around a vertical axis through its center of mass (28.65 kg.m^2 or 97900 lb.in^2) and d is the distance from the center of the platform to the springs (381 mm, or 15”). This leads to k_{shear}(6.15 Hz) = 98234 N/m (561 lb/in) and an average loss factor η_{shear}(6.15 Hz) = 1.5 %.

Similarly, mode number 3 (5.01 Hz average) is a pure vertical mode and involves almost only axial deformations of the springs. The axial stiffness at 5.01 Hz can then be extracted as

$$k_{axial}(5.01\text{ Hz}) = \frac{4\pi^2 (5.01)^2 M}{3}, \qquad (2)$$

where M is the total mass of the platform (312 lb). This leads to k_{axial}(5.01 Hz) = 46776 N/m (267 lb/in) and an average loss factor η_{shear}(6.15 Hz) = 2.2 %. This last value is in good agreement with analytical predictions.

The axial stiffness of 46776 N/m at 5.01 Hz agrees fairly well with analysis. In the absence of analytical predictions in shear, and noting that the stiffness is almost independent of frequency, the shear stiffness at 6.15 Hz can be used to calculate a ratio (which we will assume is not frequency dependent) of shear to axial stiffness

$$k_{shear} / k_{axial} \approx 2.1. \qquad (3)$$

Similarly, a ratio (assumed frequency independent) of shear to axial loss factor can be estimated as

$$\eta_{shear} / \eta_{axial} \approx 0.7. \qquad (4)$$

Those two ratios are then included in the spring property files for use in the BSC and HAM performance predictions. Analysis of the single stage platform using those ratios gives the results listed in Table 2. Agreement with experimental results is satisfactory.

The spring analysis appears to underestimate the stiffnesses by 15 to 20%, however, actual stiffnesses are expected to go down once the Viton seats are substituted for the temporary epoxy ones. Damping also appears to be underestimated by analysis as previously observed in the results of the free decay tests; this may be explained by the fact that the analysis accounts only for damping due to the internal spring structure, excluding any other effect(s).

Mode #	Nat. Frequency [Hz]		Loss Factor h = 2V[%]		Mode Shape
	MATLAB	Experiment (mean)	MATLAB	Experiment (mean)	
1	3.35	3.64	1.80	2.21	rocking around X
2	4.62	4.96	1.90	1.73	rocking around Y
3	4.66	5.01	1.94	2.19	up/down along Z
4	5.73	6.15	1.40	1.51	twist around Z
5	6.89	7.15	1.43	1.62	shear along Y
6	7.08	7.42	1.48	1.55	shear along X

Table 2: Modal parameters obtained from MATLAB model of the single stage platform compared to experimental values (using fixed ratios of shear to axial stiffnesses and loss factors).

5. Experimental Results on Fluoro-elastomer Seats

5.1 Fluoro-elastomer Seats

The geometry of those seats is very similar to that of their epoxy counterparts: they consist of a ring of solid 70 durometer Fluorel (3M type FC-2176), 71 mm OD by 47 mm ID, with a flat surface on one side and a helical ramp on the other side. A 10 mm diameter groove is part of the helical ramp is provides positive positioning for the coil. Figure ? shows a photograph of one such seat.

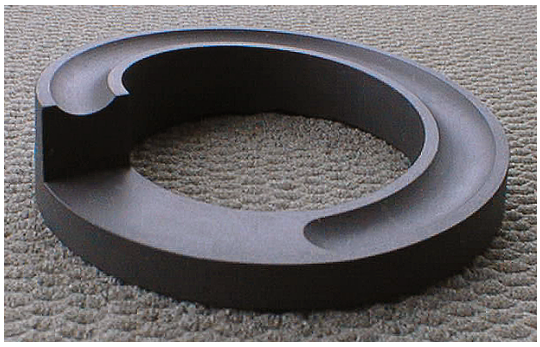

Figure 27: single stage platform test setup.

5.2 Axial Loss Factor (Free Decay Tests)

To evaluate any additional damping that may result from deformations in the high loss Fluorel material of the seat, the axial free decay tests of section 4.1 were repeated on the new seats. Some tests on epoxy seats were also repeated to separate actual differences

due to seat design from day to day variation (possibly due to small temperature variations). The results are shown in Fig. ??.

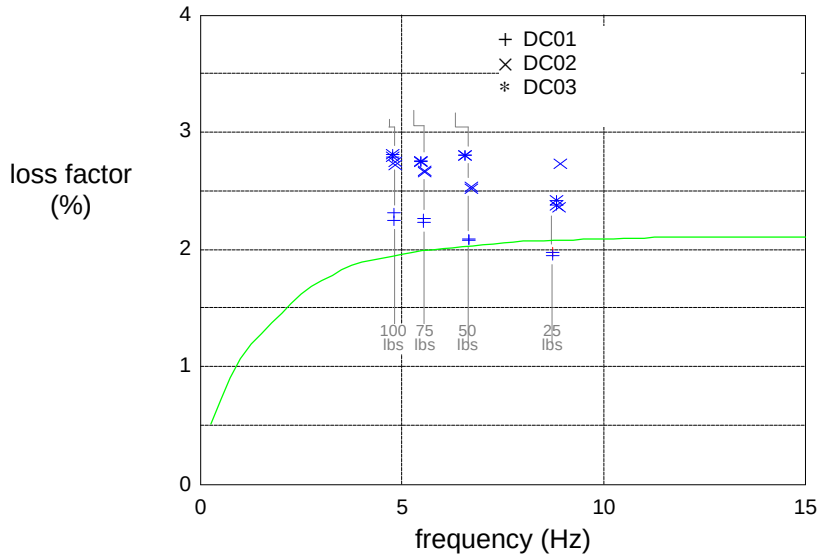

Figure 28: DC01, DC02, and DC03 damped coil prototypes - axial loss factor from free decay tests; Fluorel VS epoxy seats; analytical predictions (for stiff epoxy seats) are also shown;

5.3 Static Testing

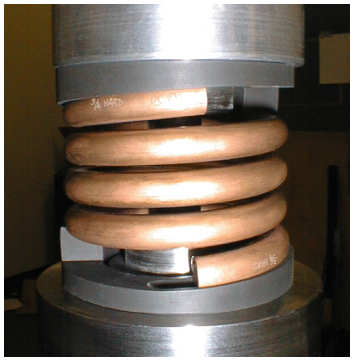

Figure 29: single stage platform test setup.

6. Concluding Remarks

This testing program is far from complete at this point. However, all experimental results on these coil springs are encouraging: they confirm analytical models for axial stiffness and damping and provide estimates of shear properties. Performance targets for stiffnesses and loss factors appear to be met.

Some design improvements are still to be incorporated and tested, in particular to resolve the issues of aluminum section axial separation and crushing of the damping layer at the outside edges of the aluminum slugs. Fabrication of more prototypes is already scheduled and will explore these problems.

Once an acceptable process is defined, further testing will investigate drift, creak, acoustic transmission, and leak tightness. Finally, pre-production quantities will be manufactured and tested to evaluate repeatability of spring properties and establish appropriate QA procedures.

7. References

1. A. M. Wahl, *Mechanical springs*, 2nd edition, McGraw-Hill Ed., 1963.
2. E. Ponslet, *Design of Vacuum Compatible Damped Metal Springs*, HYTEC Inc., document HYTEC-TN-LIGO-04a (revision *a*), January 1997.

Note 1, Linda Turner, 09/03/99 11:41:12 AM
LIGO-T970239-A-D